

Inclusive GAN: Improving Data and Minority Coverage in Generative Models

Ning Yu^{1,2}, Ke Li^{3,5,6}, Peng Zhou¹
 Jitendra Malik³, Larry Davis¹, and Mario Fritz⁴

¹ University of Maryland, College Park, United States

² Max Planck Institute for Informatics, Saarbrücken, Germany

³ University of California, Berkeley, United States

⁴ CISPA Helmholtz Center for Information Security, Saarbrücken, Germany

⁵ Institute for Advanced Study, Princeton, United States

⁶ Google, Seattle, United States

ningyu@mpi-inf.mpg.de ke.li@eecs.berkeley.edu pengzhou@cs.umd.edu
 malik@eecs.berkeley.edu lsd@cs.umd.edu fritz@cispa.saarland

Abstract. Generative Adversarial Networks (GANs) have brought about rapid progress towards generating photorealistic images. Yet the equitable allocation of their modeling capacity among subgroups has received less attention, which could lead to potential biases against underrepresented minorities if left uncontrolled. In this work, we first formalize the problem of minority inclusion as one of data coverage, and then propose to improve data coverage by harmonizing adversarial training with reconstructive generation. The experiments show that our method outperforms the existing state-of-the-art methods in terms of data coverage on both seen and unseen data. We develop an extension that allows explicit control over the minority subgroups that the model should ensure to include, and validate its effectiveness at little compromise from the overall performance on the entire dataset. Code, models, and supplemental videos are available at GitHub.

Keywords: GAN, Minority Inclusion, Data Coverage

1 Introduction

Photorealistic image generation has increasingly become reality, thanks to the emergence of large-scale datasets [9,33,47] and deep generative models [26,14,27,30]. However, these advances have come at a cost: there could be potential biases in the learned model against underrepresented data subgroups [45,55,41,15,16]. The biases are rooted in the inevitable imbalance in the dataset [38], which are preserved or even exacerbated by the generative models [55]. In particular, reconstructive (non-adversarial) generative models like variational autoencoders (VAEs) [26,37] can preserve data biases against minorities due to their objective of reproducing the frequencies images occur in the dataset, while adversarial generative models (GANs) [14,11,10] can implicitly disregard infrequent images due to the well-established problem of mode collapse [42,30], thereby further introducing model biases on top of data biases.

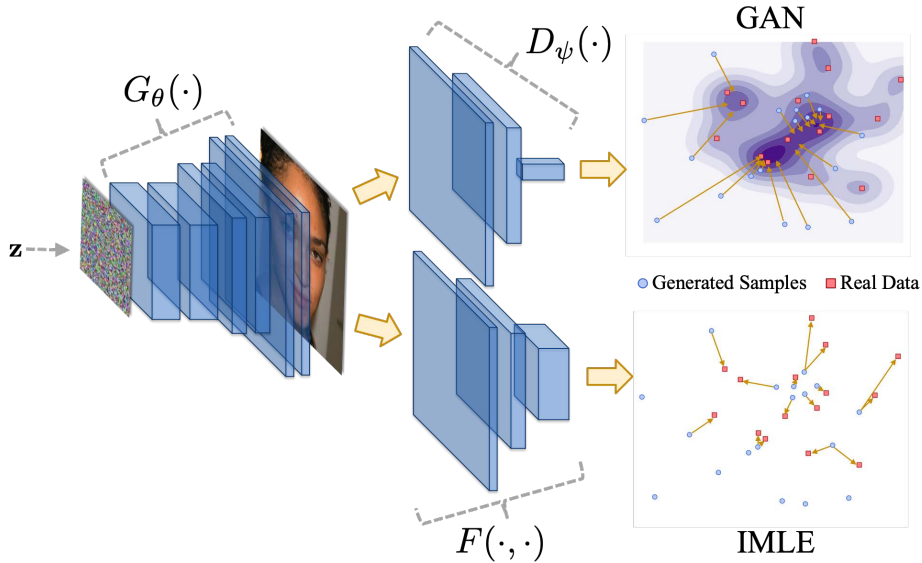


Fig. 1. The diagram of our method. It harmonizes adversarial (GAN) and reconstructive (IMLE) training in one framework without introducing an auxiliary encoder. GAN guides arbitrary sampling towards generating realistic appearances approximate to some real data while IMLE ensures data coverage where there are always generated samples approximate to each real data. See Section 3.3 for more details where G_{θ} and D_{ψ} represent the trainable generator and discriminator in a GAN, and F represents a distant metric, in some cases, a pre-trained neural network.

In this work, we aim to improve the *comprehensive* performance of the state-of-the-art generative models, with a specific focus on their coverage of minority subgroups. We start with an empirical study on the correlation between data biases and model biases, and then formalize the objective of alleviating model bias in terms of improving data coverage, in particular over the minority subgroups. We propose a new method known as IMLE-GAN that achieves competitive image quality while ensuring improved coverage of minority groups.

As its name suggests, our method harmonizes adversarial and reconstructive generative models, in the process reaping the benefits of both. Adversarial models have evolved to be the basis of many photorealistic generative models, whereas reconstructive models offer guarantees on coverage of all data points in the training dataset. We build upon one of the state-of-the-art implementations of adversarial models, i.e., StyleGAN2 [24], and incorporate it with the Implicit Maximum Likelihood Estimation (IMLE) framework [30], which is at its core reconstructive. See Figure 1 for a diagram. Different from the existing hybrid generative models, e.g., VAEGAN [27] or VEEGAN [42], that require training auxiliary networks like an encoder or a reconstructor alongside a vanilla GAN, our method operates purely with the standard components of a GAN, namely a generator and a discriminator. This brings several benefits: (1) it sidesteps the

complication from combining the minimax objective used by adversarial models and the pure minimization objective used by reconstructive models, (2) it avoids carrying over the practical issues of training auxiliary encoder models, like posterior collapse, which can cause the regression-to-the-mean problem, leading to blurry images, and (3) it obviates the need to design an encoder architecture, which is nontrivial because it must be made sufficiently flexible to be capable of approximately inverting the generator. We validate our method with thorough experiments and demonstrate more stable training and more comprehensive data coverage that go beyond what are attained by existing state-of-the-art methods. Additionally, our method is more flexible and can be easily adapted to ensure the inclusion of specified minority subgroups, which cannot be easily achieved in the context of existing methods.

Contributions. We summarize our main contributions as follows: (1) We propose the first study to formalize underrepresented minority inclusion as a data coverage problem in generative modeling; (2) We initiate a novel paradigm of harmonizing adversarial and reconstructive modeling for improving data coverage; (3) Our experiments set up a new suite of state-of-the-art performance in terms of covering both seen and unseen data; (4) We develop an effective extension of our technique to ensure inclusion of the specified minority subgroups.

2 Related Work

Bias mitigation efforts for machine learning. Bias in machine learning results from data imbalance, which can be detected and alleviated by three categories of approaches: The pre-process approaches that purify data from bias before training [7,12,13,51], the in-process approaches that enforce fairness during training with constraints or regularization in the objectives [22,49,38,53], and the post-process approaches that adjust the output from a learned model [21,18]. A comprehensive survey [34] articulates this taxonomy. These approaches target biases in classification and cannot be adapted to generative modeling.

Bias mitigation efforts for generative models. There have been relatively few papers [45,55,41,15,16] that focus on biases in generative models. [45,41,15], motivated from benefiting a downstream classifier, mainly aim for fair generation conditioned on attribute inputs, in terms of yielding allocative decisions and/or removing the correlation between generation and attribute conditions. [55] focuses on understanding the inductive bias so as to investigate the generalization of generative models. [16] proposes an importance weighting strategy to compensate for the biases of learned generative models. Different from their goals and solutions that equalize performance across different data subgroups possibly at the cost of overall performance, we instead aim to improve the overall data coverage, with a specific purpose of ensuring more significant gains over the underrepresented minorities.

Data coverage in GANs. GANs are finicky to train because of the minimax formulation and the resulting instability caused by alternating gradient ascent-descent. In addition, GANs are known to exhibit mode collapse, where the generator only learns to generate a subset of the modes of the underlying data

distribution. This commonly results in poor coverage of training data, and especially the training data of minority groups because they correspond to the less prominent modes. To alleviate mode collapse in GANs, some methods propose to improve the minimax loss function [35,2,17,1], some methods apply constraints or regularization terms along with the minimax objectives [8,5,46,32], and some other methods aim to modify the discriminator designs [44,54,36]. These directions are orthogonal to our research while, in principle, demonstrate less effective data coverage than the hybrid models below.

Data coverage in hybrid generative models. Reconstructive (non-adversarial) generative models like variational autoencoders (VAEs) [26,37], on the other hand, are more successful at data coverage because they explicitly try to maximize a lower bound on the likelihood of the real data. The likelihood is defined as the product of the probability densities assigned by the generative model to every real data point. Failing to generate even one of the data points will be heavily penalized because the density assigned to that data point will be zero, leading to the overall likelihood of all the data becoming zero.

This motivates a variety of designs for hybrid models that combine reconstruction and adversarial training. VAEGAN [27] is trained to reconstruct discriminator features instead of pixels. ALI [11] and BiGAN [10] propose to instead jointly match the bidirectional mappings between data and latent distributions. VEEGAN [42] is designed with reconstruction in the latent space, in the purpose of avoiding the metric dilemma in the data space. Hybrid models benefit for mode coverage, but deteriorate generation fidelity in practice, because of their dependency on auxiliary encoder networks. In particular, in VAEGAN [27] the generator is trained on latent vectors that are sampled from an encoded posterior, and is never trained on natural prior. At test time, only the prior is available, resulting in a mismatch between training and test conditions. In VEEGAN [42] the generator is trained jointly with a downstream encoder. The generator is guided by multiple objectives including reconstruction and data distribution approximation, while the encoder is guided only by the reconstruction objective. As a result, the back-propagation from latent reconstruction is mainly absorbed by the encoder and largely diminished before updating the generator. That leads to a mode-collapsed generator and the encoder is overfit to map an incomplete set of data modes to the full latent space. On the other hand, our method follows the idea of hybrid models, but fundamentally differs in paradigm. We propose to avoid an encoder network and instead apply all training back-propagation through the generator. A recent non-adversarial generative framework, Implicit Maximum Likelihood Estimation (IMLE) [30], satisfies our design. We discuss more about the advantages of IMLE in Section 3.2.

3 Inclusive GAN for Data and Minority Coverage

Our method is based on the idea of fusing the strengths of adversarial and reconstructive generative models. Adversarial models like generative adversarial nets (GANs) [14] have perhaps been the most thoroughly explored in the literature and therefore have yielded optimized backbone architectures that have successfully achieved photorealistic image quality [24]. Yet, the objective for training

adversarial models, the minimax objective, is known to lead to *mode collapse*, where only a subset of the data, the relatively common one, is modeled by the generator. This issue is particularly acute from the perspective of minority inclusion, because training data associated with minority subgroups by definition do not form dominant modes, and so are likely to be ignored by the generative model. Consequently, the original biases in the data could be amplified by the model: data from minority groups are rare to begin with, and would not be capable of being produced by the generative model at all due to mode collapse.

On the other hand, reconstructive models like variational autoencoders (VAEs) [26,37] and Implicit Maximum Likelihood Estimation (IMLE) [30] are often accompanied by theoretical guarantees on data coverage. Most methods are based on maximizing an approximation (usually a lower bound) to the log-likelihood of the data. Because the likelihood of the data is the product of probability densities the generative model assigns to each data point in the training set, even ignoring a single data point (i.e.: dropping the mode the data point belongs to) will have drastic consequences – not being able to generate the data point corresponds to the case when the model assigns zero density to the data point. In this case, the likelihood of the data will become zero, since one of its factors is zero. Therefore, maximizing a lower bound on the log-likelihood must prevent mode collapse and, as a result, ensure coverage of all data points.

We aim to leverage this key property of reconstructive models to achieve better data coverage in GANs. This property of reconstructive models perfectly complements the key shortcoming of adversarial models, namely the tendency to ignore under-represented data, which often comes from minority groups. To this end, we propose to harmonize GANs with the recently introduced reconstructive method of IMLE, which we call IMLE-GAN.

For completeness, we start with reviewing the basics of GANs and IMLE in Section 3.1 and 3.2 respectively. We then articulate in Section 3.3 the novel paradigm of harmonizing GAN with IMLE that avoids mode collapse, as well as the straightforward adaptation to improve minority inclusion.

3.1 Adversarial Generation: GANs

Photorealistic image generation can be viewed as the problem of sampling from the probability distribution of real-world images. To leverage the expressive power of deep learning, the sampling procedure is chosen to be a deep neural network with random noise as input. Learning the parameters of the neural network is challenging because (1) the distribution of samples generated by the neural net does not, in general, have a computationally tractable density and (2) the distribution of real-world images is unknown and so cannot be directly compared to the distribution of fake samples. Generative Adversarial Networks (GANs) [14] introduce an elegant workaround by formulating density estimation as a discriminative classification problem, and enables supervised learning methods to be used for this task.

A GAN consists of two deep neural networks: a generator $G_\theta : \mathbb{R}^d \mapsto \mathbb{R}^D$ and a discriminator $D_\psi : \mathbb{R}^D \mapsto [0, 1]$. The generator maps a latent noise vector $\mathbf{z} \sim \mathcal{N}(\mathbf{0}, \mathbf{I}_d)$ to an image, and the discriminator predicts the probability that

the image it sees is real. The real ground truth images are denoted as $\mathbf{x} \sim \hat{p}(\mathbf{x})$, sampled from an unknown distribution $\hat{p}(\mathbf{x})$. The discriminator is trained to maximize classification accuracy while the generator is trained to produce images that can fool the discriminator. More precisely, the objective is shown in Eq. 1:

$$\min_{\theta} \max_{\psi} L^{adv}(\theta, \psi) = \mathbb{E}_{\mathbf{x} \sim \hat{p}(\mathbf{x})} [\log D_{\psi}(\mathbf{x})] + \mathbb{E}_{\mathbf{z} \sim \mathcal{N}(\mathbf{0}, \mathbf{I}_d)} [\log(1 - D_{\psi}(G_{\theta}(\mathbf{z})))] \quad (1)$$

Unfortunately, GANs are unstable to train and suffer from mode collapse. Intuitively, while each generated sample is made similar to a mode in the distribution of real images, there may be modes that no generated sample is made similar to. In other words, while each generated sample gets to pick a mode it is drawn to, each mode does not get to pick a generated sample. After training, the generator will not be able to generate samples around the “unpopular” modes.

Minority modes are precisely the “unpopular” modes that are more likely to be collapsed, because there are fewer training examples corresponding to them and as a result, they are harder to generate. As shown in Section 4.3 and Figure 2, minority subgroups with diverse appearances indeed bring more challenges to generative modeling and are allocated worse coverage compared to the other subgroups.

Therefore, we leverage ideas from reconstructive models to improve the coverage of minority subgroups.

3.2 Reconstructive Generation: IMLE

Our novel paradigm is based on a recent reconstructive framework, Implicit Maximum Likelihood Estimation (IMLE) [30], that favors complete mode coverage. IMLE avoids mode collapse by reversing the direction in which generated samples are matched to real modes. In GANs, each generated sample is effectively matched to a real mode. In IMLE, each real mode is matched to a generated sample. This ensures that all real modes, including each underrepresented minority mode, are matched, and no real mode is left out.

Mathematically, IMLE tackles the optimization problem in Eq. 2:

$$\min_{\theta} \mathbb{E}_{\mathbf{z}_1, \dots, \mathbf{z}_m \sim \mathcal{N}(\mathbf{0}, \mathbf{I}_d)} \left[\mathbb{E}_{\mathbf{x} \sim \hat{p}(\mathbf{x})} \left[\min_{i \in \{1, \dots, m\}} \|G_{\theta}(\mathbf{z}_i) - \mathbf{x}\|_2^2 \right] \right] \quad (2)$$

The joint optimization is achieved by alternating between the two decoupled phases until convergence. The first phase corresponds to the inner optimization, where we search for each \mathbf{x} the optimal $\mathbf{z}^*(\mathbf{x})$ from the latent vector candidates, given a fixed G_{θ} . This is implemented by the Prioritized DCI [29], a fast nearest neighbor search algorithm. The second phase corresponds to the outer optimization, where we train the generator in the regular back-propagation manner, given pairs of $(\mathbf{x}, \mathbf{z}^*(\mathbf{x}))$.

One significant advantage of IMLE over the other reconstructive models is the elimination of the need for an auxiliary encoder. The encoder encourages mode coverage but at the cost of either deviating the latent sampling distribution from the original prior (in VAEGAN [27]) or absorbing the training gradients before substantially back-propagating to the generator (in VEEGAN [42]). Unlike

them, IMLE directly samples latent vector from a natural prior during training and encourages explicit reconstruction fully upon the generator. When combining with adversarial loss as described in Section 3.3, it sheds the light to more effective training than VEEGAN [42] as well as higher generation fidelity than VAEGAN [27] at test time (when only the prior is available). See Section 4.5, Table 2, and Figure 3 for the advantageous performance of our IMLE-GAN. Several follow-up works, e.g., GLANN [20] and conditional IMLE [31], also validate the improved effectiveness of IMLE framework in a reconstructive generation context.

3.3 Harmonizing Adversarial and Reconstructive Generation: IMLE-GAN

IMLE pursues data coverage by explicitly maximizing the likelihood of the data. The advantage is to enhance data approximation by matching each data point with a latent vector. However, the downside is equally obvious: the finite and discrete data observations match to a finite and discrete set of latent vectors, which ignores the generalization over the continuous latent space. That motivates us to bring back the desirable generalization characteristics of GANs. Therefore, we propose the first attempt to harmonize adversarial training into IMLE framework, that targets to ensure both generation quality (precision) and coverage (recall) simultaneously.

The vanilla hybrid model between IMLE and GAN is to directly add the adversarial loss in Eq. 1 to the optimization in Eq. 2. However, that may lead to the risk of further unstable training due to two key distinctions between the adversarial loss and the reconstruction loss. First, the two losses have different sampling supports. The reconstruction loss is supported only on the discrete and sparse matching latent vectors $\mathbf{z}^*(\mathbf{x})$ while the adversarial loss is supported on the continuous latent space $\mathbf{z} \sim N(0, \mathbf{I}_d)$. Second, the two losses work in different metric spaces. The reconstruction loss is explicitly formulated as the sample-wise posterior regression in the pixel Euclidean space, while the adversarial loss is implicitly formulated as the Jensen-Shannon divergence between two probabilistic distributions.

To bridge the gap in losses, we propose two adaptations that benefit for harmonizing between GAN and IMLE. First, to make the reconstruction more densely supported, we augment the matching latent vectors with interpolation. The benefits of interpolation-based data augmentation are validated by previous works in both discriminative modeling [50,4] and generative modeling [3,48]. Second, to make the metric spaces of the two losses more comparable, we measure the reconstruction loss in a deep feature space instead of pixel space, such that the back-propagation from a deep metric contains a comparable amount and level of information to that from the discriminator. Mathematically, we optimize Eq. 3 until convergence:

$$\min_{\theta} \max_{\psi} L^{adv}(\theta, \psi) + \mathbb{E}_{\mathbf{z}_1, \dots, \mathbf{z}_m \sim \mathcal{N}(\mathbf{0}, \mathbf{I}_d)} [\lambda L^{rec}(\theta) + \beta L^{itp}(\theta)] \quad (3)$$

Here $L^{adv}(\theta, \psi)$ is as defined in Eq. 1, and

$$L^{rec}(\theta) = \mathbb{E}_{\mathbf{x} \sim \hat{p}(\mathbf{x})} [F(G_\theta(\mathbf{z}^*(\mathbf{x})), \mathbf{x})] \quad (4)$$

$$L^{itp}(\theta) = \mathbb{E}_{\mathbf{x}, \tilde{\mathbf{x}} \sim \hat{p}(\mathbf{x}), \alpha \sim U[0,1]} [\alpha F(G_\theta(\mathbf{z}^*(\alpha, \mathbf{x}, \tilde{\mathbf{x}})), \mathbf{x}) + (1 - \alpha) F(G_\theta(\mathbf{z}^*(\alpha, \mathbf{x}, \tilde{\mathbf{x}})), \tilde{\mathbf{x}})] \quad (5)$$

$$\mathbf{z}^*(\mathbf{x}) = \arg \min_{i \in \{1, \dots, m\}} F(G(\mathbf{z}_i), \mathbf{x}) \quad (6)$$

$$\mathbf{z}^*(\alpha, \mathbf{x}, \tilde{\mathbf{x}}) = \alpha \mathbf{z}^*(\mathbf{x}) + (1 - \alpha) \mathbf{z}^*(\tilde{\mathbf{x}}) \quad (7)$$

Eq. 4 corresponds to the inner expectation in Eq. 2 and Eq. 6 corresponds to the inner optimization in Eq. 2. Eq. 7 expresses the linear interpolation between two matched latent vectors from Eq. 6, weighted by an arbitrarily sampled factor α . Eq. 5 expresses the linear interpolation between two reconstruction losses, weighted by the same factor α . λ and β are used to balance each loss term. $F(\cdot, \cdot)$ is a distance metric with four options: ℓ_2 distance in the pixel space, in the discriminator feature space [27], in the Inception feature space [40], and by a deep similarity metric LPIPS [52]. We experimented with each and report results in Section 4.4.

3.4 Minority Coverage in IMLE-GAN

IMLE-GAN framework is designed for improving the overall mode coverage. More advantageously to the other hybrid models, it is also straightforward to adapt to minority inclusion. We simply need to replace the entire dataset $\hat{p}(\mathbf{x})$ with a specified minority subgroup $\hat{q}(\mathbf{y}) \subseteq \hat{p}(\mathbf{x})$ in Eq. 4 and Eq. 5 (for reconstructive training) and leave Eq. 1 unchanged (for adversarial training). This ensures an explicit coverage over the minority while still carrying out the approximation to the entire real data. There is an additional side advantage of this adaptation. Because $\hat{q}(\mathbf{y})$ is in practice a much smaller set than $\hat{p}(\mathbf{x})$ with less data imbalance and variance, covering $\hat{q}(\mathbf{y})$ should be easier with higher performance. We summarize our IMLE-GAN algorithm with minority inclusion in the supplementary material.

4 Experiments

We first articulate the experimental setup in Section 4.1. In Section 4.2 we start with preliminary validation on Stacked MNIST dataset [35], an easy and interpretable task. In Section 4.3 we conduct empirical study to analyze the correlation between data bias and model bias. We then move on to Section 4.4 for the validation of our two harmonization strategies. In Section 4.5 we perform comprehensive evaluation and comparisons on CelebA dataset [33], and finally specify minority inclusion applications in Section 4.6.

4.1 Setup

Datasets. For preliminary study, we employ Stacked MNIST dataset [35] for explicit data coverage evaluation. It is derived from the standard MNIST dataset [28] with an increased number of discrete modes. 240,000 RGB images in the size of 32×32 are synthesized by stacking three random digit images from MNIST

along the color channel, resulting in 1,000 explicit modes in a uniform distribution corresponding to the number of possible triples of digits.

For further comprehensive study in the practical purpose of minority inclusion, we conduct most of the experiments on CelebA human face dataset [33], where the 40 binary facial attributes are used to specify minority subgroups. We sample the first 30,000 images in the size of 128×128 for GAN training, and sample the last 3,000 or 30,000 images for validation. The image cropping process refers to [23].

GAN backbone. We build our IMLE-GAN framework wrapping the most recent state-of-the-art StyleGAN2 [24] for unconditional image generation. We reuse all their default settings except that we set the output size of a generator to $32 \times 32 \times 3$ for Stacked MNIST and $128 \times 128 \times 3$ for CelebA. All the other hyperparameter settings related to IMLE-GAN implementation are in the supplementary material.

Baseline methods. Besides the backbone StyleGAN2 [24], we also compare our method to six previous techniques that show improvement in data coverage and/or generation diversity: SNGAN [36], DSGAN [46], PacGAN [32], ALI [11], VAEGAN [27], VEEGAN [42]. For fair comparisons, we replace their original network architectures with the ones from StyleGAN2. For ALI, VAEGAN, and VEEGAN where an encoder is involved, we adapt the discriminator architecture for the encoder. See supplementary material for their parameter settings.

Evaluation. For the Stacked MNIST dataset with 1,000 uniform discrete modes, following [35,42], we report the number of generated modes that is detected by a pre-trained mode classifier, as well as the KL divergence between the generated mode distribution and the uniform distribution. The statistics are calculated from 240,000 randomly generated samples.

For unconditional general image generation, e.g. on CelebA, Fréchet Inception Distance (FID) [19] is a commonly used metric and is the major pursuit of most generative models. It reflects both data quality (precision) and coverage (recall) but entangles them implicitly using the mean and standard deviation of Inception features [43] of generated samples. We also explicitly measure the Precision and Recall [39] of a generative model w.r.t. the real dataset in the Inception space. Moreover, to emphasize on instance-level data coverage evaluation, we further involve Inference via Optimization Measure (IvOM) [35] into our metric suite, which measures the mean retrieval error from a generative model given each query image. In our experiments, the retrieval is implemented as an optimization w.r.t. the latent vector, such that a learned generator approximates its generation towards the query image. The retrieval error is then calculated as the difference between the optimal generated image and the query image. The optimization objective and the error are measured using the deep similarity metric LPIPS [52]. We also report the standard deviation of IvOM across 40 CelebA attributes, in order to evaluate the balance of generative coverage. For the generalization purpose, we evaluate on both the training set and a validation set (unseen during training). More details of the evaluation implementation are in the supplementary material.

Table 1. Comparisons on Stacked MNIST dataset. The statistics are calculated from 240,000 randomly generated samples. We indicate for each metric whether a higher (\uparrow) or lower (\downarrow) value is more desirable. We highlight the best performance in **bold**.

	# modes (max 1000) (\uparrow)	KL to uniform (\downarrow)
StyleGAN2 [24]	940	0.424
SNGAN [36]	571	1.382
DSGAN [46]	955	0.343
PacGAN [32]	908	0.638
ALI [11]	956	0.680
VAEGAN [27]	929	0.534
VEEGAN [42]	987	0.310
Ours LPIPS interp	997	0.200

4.2 Preliminary Study on Stacked MNIST

In a real-world data distribution, the notion of modes is difficult to quantize. We instead start with Stacked MNIST [35] where a large number of discrete modes are unambiguously synthesized. This allows us to zoom in the challenge of mode collapse and facilitate a precise pre-validation.

We report the evaluation in Table 1. Our method narrows down the gap between experimental performance and the theoretical limit: It covers the most number of modes and achieves the closest mode distribution to the uniform distribution ground truth. This study validates the improved effectiveness of harmonizing IMLE with GAN, compared to the other GAN models or hybrid models, in terms of explicit mode/data coverage. This sheds the light and pre-qualifies to apply our method on more complicated real-world datasets.

4.3 Empirical Study on Data and Model Biases

As discussed in Section 2, data biases lead to biases in generative models. Even worse, a model without attention to minorities can exacerbate such biases against allocating adequate representation capacities to them. In this empirical study, we first show the existence of biases across CelebA attributes in terms of sample counts and sample variance, and then correlate them to the biased performance of the backbone StyleGAN2 [24].

As shown in the left barplot of Figure 2, given the attribute histogram over 30,000 samples, 29 out of 40 binary attributes are more than 50% biased from the balance point (15,000 out of 30,000 samples with a positive attribute annotation, shown as the red dashed line). The extreme case is for the *Bald* attribute where the positive samples count for only 2% of the population. On the other hand, in the right barplot of Figure 2, we calculate the standard deviation of Inception features [40] of samples within each attribute, and notice a wide range spanning from 0.038 to 0.062. The maximum is almost double to the minimum.

Too few samples or too large appearance variance in one attribute discourages generative coverage for that attribute, and thus results in biases. To quantify the per-attribute coverage, we measure the mean IvOM [35] over training samples that have such a positive attribute. A larger value indicates a worse coverage.

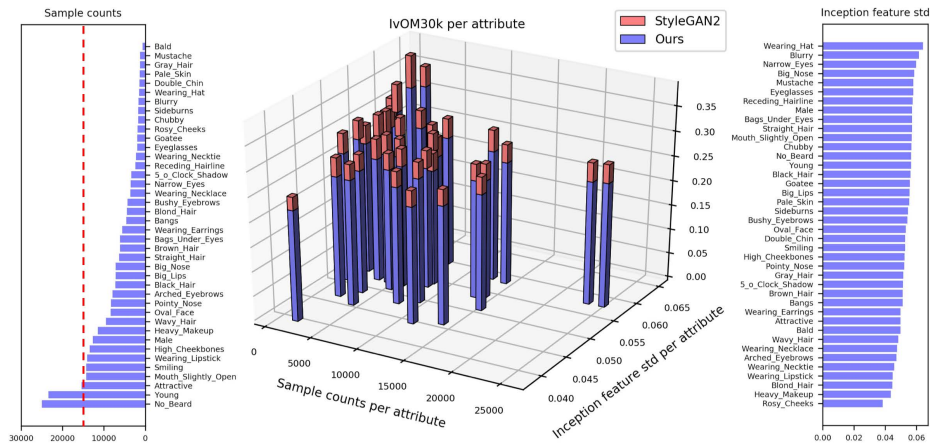


Fig. 2. Visualizations for data and model biases. Left: Sorted CelebA attribute histogram with a balance point marked by the red dashed line. Right: Sorted Inception feature variance per attribute. Middle: Per-attribute mean IvOM measurements over 30,000 CelebA training samples for StyleGAN2 (red) and for our method (blue), where each bar corresponds to one attribute.

In the middle barplot of Figure 2, we visualize the correlation between IvOM and the joint distribution of sample counts and sample variance. There is a clear gradient trend of IvOM when the samples of an attribute turn rarer and/or more diverse. To validate such a strong correlation, we first normalize the sample counts and sample variance across attributes by their means and standard deviations. Then we simply add them up as a joint variable vector, and calculate its Spearman’s ranking correlation to the per-attribute IvOM. For StyleGAN2 (the red bar in Figure 2), the correlation is 0.75, indicating a strong correlation between data biases and model biases. This evidences the urgency to mitigate biases against the rare and diverse samples, in another word, to enhance the coverage over minority subgroups.

4.4 Effectiveness of Harmonization

In Section 3.3 we propose two strategies to harmonize adversarial and reconstructive training: the deep distance metric and the interpolation-based augmentation. We compare four distance metrics and with/without augmentation in the third part of Table 2. The radar plots in [Row2, Col2] - [Row2, Col6] of Figure 3 assist interpret the table. For distance metrics, the pixel space (the vanilla version) achieves the desirable Recall and the Inception space achieves the desirable FID, but they contain obvious shortcomings in the other metrics. In contrast, the LPIPS similarity shows near-top measures all around with the most balanced performance, which will be employed in our full method. For augmentation, it consistently benefits for all the measures based on LPIPS, which will also be employed. In summary, both of our strategies play beneficial roles in harmonizing GAN and IMLE that effectively improve the overall performance (including data coverage) from the vanilla version.

Table 2. Comparisons on CelebA dataset. We indicate for each metric whether a higher (\uparrow) or lower (\downarrow) value is more desirable. For the generalization purpose, we measure on both the training dataset (“Train”) and a disjoint validation dataset (“Val”). The third part of the table corresponds to our harmonization strategies in Section 4.4 and the forth (last) part corresponds to our minority inclusion model variants in Section 4.6. We highlight the best performance in **bold** and the second best performance with underline, excluding the last part of the table. For an easier interpretation, we visualize in Figure 3 the comprehensive evaluation over the validation set.

Method	FID30k		Precision30k		Recall30k		IvOM3k		IvOM3k std	
	\downarrow	\downarrow	\uparrow	\uparrow	\uparrow	\uparrow	\downarrow	\downarrow	\downarrow	\downarrow
	Train	Val	Train	Val	Train	Val	Train	Val	Train	Val
StyleGAN2 [24]	9.37	9.49	0.855	0.844	0.730	0.741	0.303	0.302	0.0268	0.0264
SNGAN [36]	13.32	13.24	0.792	0.787	0.631	0.616	0.325	0.322	0.0274	0.0261
DSGAN [46]	14.29	14.00	0.868	0.862	0.679	0.724	0.301	0.300	0.0227	0.0220
PacGAN [32]	15.05	15.12	0.870	0.869	0.726	0.758	0.311	0.308	0.0256	0.0238
ALI [11]	<u>10.09</u>	<u>10.06</u>	0.842	0.867	0.688	0.710	0.298	0.297	0.0240	0.0245
VAEGAN [27]	18.26	18.14	0.738	0.733	0.782	0.779	0.310	0.307	0.0264	0.0246
VEEGAN [42]	16.34	16.13	0.752	0.768	0.660	0.695	0.260	0.269	<u>0.0190</u>	0.0181
Ours pixel	32.54	31.82	0.828	0.828	0.882	0.879	0.265	0.277	0.0207	0.0231
Ours Dfeature [27]	22.38	21.92	0.849	0.842	0.806	0.826	0.263	0.277	0.0189	0.0219
Ours Inception [40]	11.62	11.61	0.843	0.861	0.704	0.712	0.301	0.303	0.0234	0.0249
Ours LPIPS [52]	12.30	12.10	<u>0.916</u>	<u>0.936</u>	0.835	0.843	<u>0.256</u>	<u>0.263</u>	0.0194	<u>0.0195</u>
Ours LPIPS interp	11.56	11.28	0.927	0.941	<u>0.849</u>	<u>0.848</u>	0.255	0.262	0.0193	<u>0.0195</u>
Ours <i>Eyeglasses</i>	13.54	14.43	0.914	0.910	0.890	0.895	0.255	0.265	0.0249	0.0193
Ours <i>Bald</i>	13.34	13.46	0.903	0.895	0.886	0.892	0.268	0.272	0.0381	0.0227
Ours <i>EN&HM</i>	15.18	15.00	0.885	0.891	0.830	0.842	0.268	0.270	0.0318	0.0277
Ours <i>BUE&HC&A</i>	14.27	13.85	0.878	0.874	0.871	0.884	0.262	0.266	0.0300	0.0254

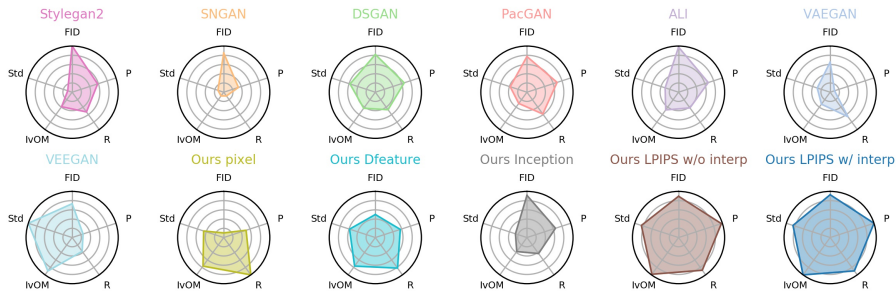


Fig. 3. Radar plots of the first three parts of Table 2. “P” represents Precision, “R” represents Recall, and “Std” represents IvOM standard deviation. Values have been normalized to the unit range, and axes are inverted so that the higher value is always better.

4.5 Comparisons on CelebA

To evaluate our data coverage performance in practice, we conduct comprehensive comparisons on CelebA [33] against several baseline methods that design

for data coverage and/or generation diversity. The first three parts of Table 2 show our comparisons. Figure 3 assists interpret the table. We find:

(1) FID is not a gold standard to reflect the entire capability of a generative model, as it ranks differently from the other metrics.

(2) Compared to the original backbone StyleGAN2 which achieves the best FID, our full method (“Ours LPIPS interp”) trades slight FID deterioration for significant boosts in all the other metrics. This is a meaningful trade-off because precision (FID) can be traded back with recall (Recall, IvOM) via the truncation trick used in [6,24], while the inverse direction is infeasible.

(3) Our method outperforms all the existing state-of-the-art techniques in terms of Precision, Recall, and IvOM, where the latter two are the key evidence for effective data coverage. The last radar plot in Figure 3 shows our method achieves near-top measures all around with the most balanced performance.

(4) Our method also achieves the top-3 performance in the standard deviation of per-attribute IvOM, indicating an equalized capacity across the attribute spectrum, compared to the original StyleGAN2. The blue bars in the middle barplot of Figure 2 also visualize our method consistently outperforms StyleGAN2 for all the attributes, in particular with more significant improvement for the more underrepresented minority subgroups.

(5) Figure 4 shows qualitative comparisons in terms of query retrieval and uncurated random generation. Our method responds correctly to the query attributes (hat, sunglasses, etc.) as well as demonstrates desirable generation fidelity and diversity.

(6) All the conclusions above generalize well to unseen data, as evidenced by the “Val” columns in Table 2.

4.6 Extension to Minority Inclusion

Encouraged by the significant improvement in overall data coverage, we adapt our method with specific coverage over minority subgroups, so as to ensure explicit inclusion during generative modeling (See our algorithm in the supplementary material). Without introducing unconscious bias on the CelebA attributes, in the experiments, we arbitrarily specify four sets of attributes, the samples of which count for no more than 6% of the population, and therefore, constitute four minority subgroups respectively. The attribute sets and their portions are listed in the first column of Table 3.

To validate the minority inclusion, we first compare our minority model variants over the corresponding minority subsets against the backbone StyleGAN2 and against our general full model. See Table 3 for the results. Our minority variants consistently outperform the two baselines over varying minority subgroups. In Figure 5, our method retrieves the minority attributes the most accurately, even for the subtle attributes like eye bags. It validates better training data utilization of our minority models. Additional results are shown in the supplementary material and supplementary videos.

To validate the overall performance beyond the minority subgroups, we further attach in the last part of Table 2 the performance on the entire attribute spectrum. We conclude that the improvement of all of our minority models on

Table 3. Comparisons on CelebA minority subgroups, where the percentages show their portion w.r.t. the entire population. The metrics are measured on the corresponding subgroups only. We indicate for each metric whether a higher (\uparrow) or lower (\downarrow) value is more desirable. For the generalization purpose, we measure on both the training dataset (“Train”) and a disjoint validation dataset (“Val”). We highlight the best performance in **bold**.

Arbitrary minority subgroup	Method	Precision1k minority only		Recall1k minority only		IvOM1k minority only	
		\uparrow		\uparrow		\downarrow	
		Train	Val	Train	Val	Train	Val
<i>Eyeglasses</i> (6%)	StyleGAN2 [24]	0.719	0.704	0.582	0.589	0.355	0.352
	Ours LPIPS interp	0.843	0.845	0.740	0.708	0.309	0.308
	Ours <i>Eyeglasses</i>	0.904	0.919	0.897	0.892	0.261	0.288
<i>Bald</i> (2%)	StyleGAN2 [24]	0.707	0.750	0.461	0.424	0.301	0.305
	Ours LPIPS interp	0.763	0.783	0.666	0.670	0.269	0.273
	Ours <i>Bald</i>	0.779	0.718	0.842	0.810	0.189	0.273
<i>Narrow_Eyes & Heavy_Makeup</i> (4%)	StyleGAN2 [24]	0.719	0.701	0.543	0.577	0.272	0.274
	Ours LPIPS interp	0.794	0.760	0.632	0.621	0.246	0.248
	Ours <i>EN&HM</i>	0.799	0.766	0.698	0.696	0.194	0.244
<i>Bags_Under_Eyes & High_Cheekbones & Attractive</i> (4%)	StyleGAN2 [24]	0.838	0.804	0.736	0.725	0.263	0.268
	Ours LPIPS interp	0.816	0.831	0.700	0.742	0.237	0.241
	Ours <i>BUE&HC&A</i>	0.889	0.883	0.813	0.809	0.191	0.237

their minority subgroups is at little or no compromise from their performance on the overall dataset.

5 Conclusion

We have presented the first study that formalizes the problem of minority inclusion as one of data coverage in generative modeling. We improve data coverage using a novel paradigm that harmonizes adversarial training (StyleGAN2) with reconstructive generation (IMLE). The experiments validate that our method outperforms the existing state-of-the-art methods in terms of Precision, Recall, and IvOM over CelebA. The improvement generalizes well on unseen data. We further extend our method that ensures explicit inclusion for minority subgroups at little or no compromise from the overall performance on the entire dataset. We demonstrate this is an effective step towards more inclusive generative modeling.

Acknowledgement

This project was partially funded by DARPA MediFor program under cooperative agreement FA87501620191 and by ONR MURI (N00014-14-1-0671). We acknowledge the Maryland Advanced Research Computing Center, Max Planck Institute for Informatics, and UC Berkeley for providing computing resources. We thank Tero Karras and Michal Lukáč for sharing code. We also thank Richard Zhang and Dingfan Chen for constructive advice in general.



Fig. 4. Retrieval samples on the left (used for IvOM evaluation) and random generation samples on the right (used for FID, precision, and recall evaluation). The query images for retrieval in the top left row are real and unseen during training.

References

1. Adler, J., Lutz, S.: Banach wasserstein gan. In: NeurIPS (2018)
2. Arjovsky, M., Chintala, S., Bottou, L.: Wasserstein gan. In: ICML (2017)
3. Beckham, C., Honari, S., Verma, V., Lamb, A.M., Ghadiri, F., Hjelm, R.D., Bengio, Y., Pal, C.: On adversarial mixup resynthesis. In: NeurIPS (2019)
4. Berthelot, D., Raffel, C., Roy, A., Goodfellow, I.: Understanding and improving interpolation in autoencoders via an adversarial regularizer. In: ICLR (2018)
5. Berthelot, D., Schumm, T., Metz, L.: Began: Boundary equilibrium generative adversarial networks (2017)
6. Brock, A., Donahue, J., Simonyan, K.: Large scale gan training for high fidelity natural image synthesis. In: ICLR (2019)
7. Calders, T., Kamiran, F., Pechenizkiy, M.: Building classifiers with independency constraints. In: ICDM Workshops (2009)
8. Chen, X., Duan, Y., Houthoofd, R., Schulman, J., Sutskever, I., Abbeel, P.: Info-gan: Interpretable representation learning by information maximizing generative adversarial nets. In: NeurIPS (2016)

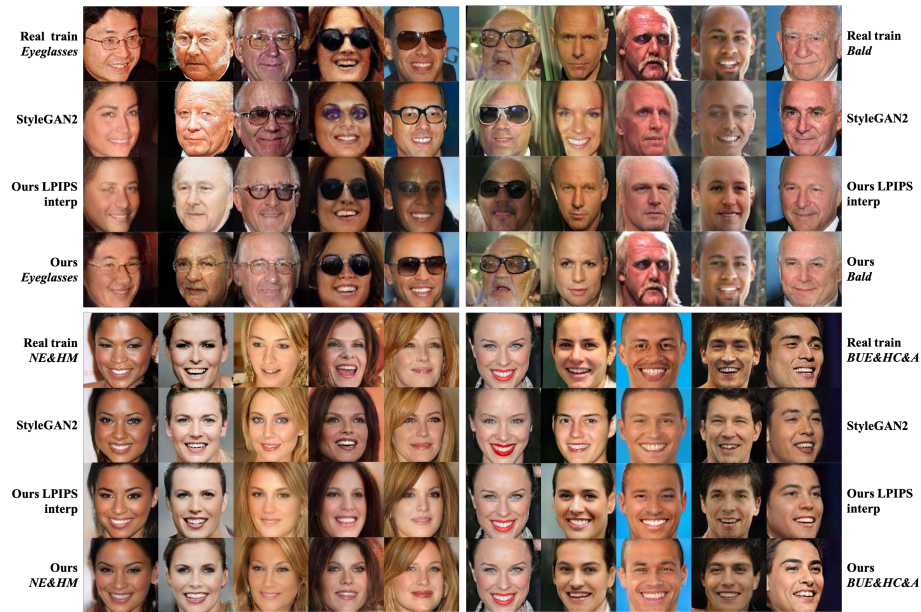


Fig. 5. Retrieval samples according to different minority subgroups. The query images for retrieval in the top row of each sub-figure are real from the training set.

9. Deng, J., Dong, W., Socher, R., Li, L.J., Li, K., Fei-Fei, L.: Imagenet: A large-scale hierarchical image database. In: 2009 IEEE conference on computer vision and pattern recognition. pp. 248–255. Ieee (2009)
10. Donahue, J., Krähenbühl, P., Darrell, T.: Adversarial feature learning. In: ICLR (2016)
11. Dumoulin, V., Belghazi, I., Poole, B., Mastropietro, O., Lamb, A., Arjovsky, M., Courville, A.: Adversarially learned inference. In: ICLR (2016)
12. Dwork, C., Hardt, M., Pitassi, T., Reingold, O., Zemel, R.: Fairness through awareness. In: Proceedings of the 3rd innovations in theoretical computer science conference (2012)
13. Feldman, M., Friedler, S.A., Moeller, J., Scheidegger, C., Venkatasubramanian, S.: Certifying and removing disparate impact. In: KDD (2015)
14. Goodfellow, I., Pouget-Abadie, J., Mirza, M., Xu, B., Warde-Farley, D., Ozair, S., Courville, A., Bengio, Y.: Generative adversarial nets. In: NeurIPS (2014)
15. Grover, A., Choi, K., Shu, R., Ermon, S.: Fair generative modeling via weak supervision. arXiv (2019)
16. Grover, A., Song, J., Kapoor, A., Tran, K., Agarwal, A., Horvitz, E.J., Ermon, S.: Bias correction of learned generative models using likelihood-free importance weighting. In: NeurIPS (2019)
17. Gulrajani, I., Ahmed, F., Arjovsky, M., Dumoulin, V., Courville, A.C.: Improved training of wasserstein gans. In: NeurIPS (2017)
18. Hardt, M., Price, E., Srebro, N.: Equality of opportunity in supervised learning. In: NeurIPS (2016)

19. Heusel, M., Ramsauer, H., Unterthiner, T., Nessler, B., Hochreiter, S.: Gans trained by a two time-scale update rule converge to a local nash equilibrium. In: *NeurIPS (2017)*
20. Hoshen, Y., Li, K., Malik, J.: Non-adversarial image synthesis with generative latent nearest neighbors. In: *CVPR (2019)*
21. Kamiran, F., Calders, T., Pechenizkiy, M.: Discrimination aware decision tree learning. In: *ICDM (2010)*
22. Kamishima, T., Akaho, S., Sakuma, J.: Fairness-aware learning through regularization approach. In: *ICDM Workshops (2011)*
23. Karras, T., Aila, T., Laine, S., Lehtinen, J.: Progressive growing of gans for improved quality, stability, and variation. In: *ICLR (2018)*
24. Karras, T., Laine, S., Aittala, M., Hellsten, J., Lehtinen, J., Aila, T.: Analyzing and improving the image quality of stylegan. *arXiv (2019)*
25. Kingma, D.P., Ba, J.: Adam: A method for stochastic optimization. In: *ICLR (2015)*
26. Kingma, D.P., Welling, M.: Auto-encoding variational bayes. In: *ICLR (2014)*
27. Larsen, A.B.L., Sønderby, S.K., Larochelle, H., Winther, O.: Autoencoding beyond pixels using a learned similarity metric. In: *ICML (2016)*
28. LeCun, Y., Bottou, L., Bengio, Y., Haffner, P.: Gradient-based learning applied to document recognition. *Proceedings of the IEEE (1998)*
29. Li, K., Malik, J.: Fast k-nearest neighbour search via prioritized dci. In: *ICML (2017)*
30. Li, K., Malik, J.: Implicit maximum likelihood estimation. *arXiv (2018)*
31. Li, K., Zhang, T., Malik, J.: Diverse image synthesis from semantic layouts via conditional imle. In: *ICCV (2019)*
32. Lin, Z., Khetan, A., Fanti, G., Oh, S.: Pacgan: The power of two samples in generative adversarial networks. In: *NeurIPS (2018)*
33. Liu, Z., Luo, P., Wang, X., Tang, X.: Deep learning face attributes in the wild. In: *ICCV (2015)*
34. Mehrabi, N., Morstatter, F., Saxena, N., Lerman, K., Galstyan, A.: A survey on bias and fairness in machine learning (2019)
35. Metz, L., Poole, B., Pfau, D., Sohl-Dickstein, J.: Unrolled generative adversarial networks. In: *ICLR (2017)*
36. Miyato, T., Kataoka, T., Koyama, M., Yoshida, Y.: Spectral normalization for generative adversarial networks. In: *ICLR (2018)*
37. Rezende, D.J., Mohamed, S., Wierstra, D.: Stochastic backpropagation and variational inference in deep latent gaussian models. In: *ICML (2014)*
38. Ryu, H.J., Adam, H., Mitchell, M.: Inclusivefacenet: Improving face attribute detection with race and gender diversity (2018)
39. Sajjadi, M.S., Bachem, O., Lucic, M., Bousquet, O., Gelly, S.: Assessing generative models via precision and recall. In: *NeurIPS (2018)*
40. Salimans, T., Goodfellow, I., Zaremba, W., Cheung, V., Radford, A., Chen, X.: Improved techniques for training gans. In: *NeurIPS (2016)*
41. Sattigeri, P., Hoffman, S.C., Chenthamarakshan, V., Varshney, K.R.: Fairness gan: Generating datasets with fairness properties using a generative adversarial network (2019)
42. Srivastava, A., Valkov, L., Russell, C., Gutmann, M.U., Sutton, C.: Veegan: Reducing mode collapse in gans using implicit variational learning. In: *NeurIPS (2017)*
43. Szegedy, C., Vanhoucke, V., Ioffe, S., Shlens, J., Wojna, Z.: Rethinking the inception architecture for computer vision. In: *CVPR (2016)*

44. Warde-Farley, D., Bengio, Y.: Improving generative adversarial networks with denoising feature matching. In: ICLR (2017)
45. Xu, D., Yuan, S., Zhang, L., Wu, X.: Fairgan: Fairness-aware generative adversarial networks. In: Big Data (2018)
46. Yang, D., Hong, S., Jang, Y., Zhao, T., Lee, H.: Diversity-sensitive conditional generative adversarial networks. In: ICLR (2019)
47. Yu, F., Zhang, Y., Song, S., Seff, A., Xiao, J.: Lsun: Construction of a large-scale image dataset using deep learning with humans in the loop. arXiv (2015)
48. Yu, N., Barnes, C., Shechtman, E., Amirghodsi, S., Lukác, M.: Texture mixer: A network for controllable synthesis and interpolation of texture. In: CVPR (2019)
49. Zafar, M.B., Valera, I., Rodriguez, M.G., Gummadi, K.P.: Fairness constraints: Mechanisms for fair classification. In: AISTATS (2017)
50. Zhang, H., Cisse, M., Dauphin, Y.N., Lopez-Paz, D.: mixup: Beyond empirical risk minimization. In: ICLR (2018)
51. Zhang, L., Wu, Y., Wu, X.: A causal framework for discovering and removing direct and indirect discrimination. In: IJCAI (2017)
52. Zhang, R., Isola, P., Efros, A.A., Shechtman, E., Wang, O.: The unreasonable effectiveness of deep features as a perceptual metric. In: CVPR (2018)
53. Zhao, J., Wang, T., Yatskar, M., Ordonez, V., Chang, K.W.: Men also like shopping: Reducing gender bias amplification using corpus-level constraints. In: EMNLP (2017)
54. Zhao, J., Mathieu, M., LeCun, Y.: Energy-based generative adversarial network. In: ICLR (2017)
55. Zhao, S., Ren, H., Yuan, A., Song, J., Goodman, N., Ermon, S.: Bias and generalization in deep generative models: An empirical study. In: NeurIPS (2018)

Algorithm 1: IMLE-GAN with Minority Inclusion

Data: Real training data $\hat{p}(\mathbf{x})$ and a specified minority subgroup $\hat{q}(\mathbf{y})$
Result: A generator G_θ with specified minority inclusion performance

```

for epoch =  $\{1, \dots, E\}$  do
  if epoch %  $S == 0$  then
    Sample  $\mathbf{z}_1, \dots, \mathbf{z}_m \sim \mathcal{N}(0, \mathbf{I}_d)$  i.i.d.;
    for  $\mathbf{y}_j \sim \hat{q}(\mathbf{y})$  do
       $\mathbf{z}^*(\mathbf{y}_j) \leftarrow \arg \min_{i \in \{1, \dots, m\}} F(G_\theta(\mathbf{z}_i), \mathbf{y}_j)$ ;
    end
  end
  for  $\mathbf{x}_k \sim \hat{p}(\mathbf{x})$  and  $\mathbf{y}_i, \mathbf{y}_j \sim \hat{q}(\mathbf{y})$  do
    Sample  $\mathbf{z} \sim \mathcal{N}(0, \mathbf{I}_d)$ ;
     $L^{adv} \leftarrow \log D_\psi(\mathbf{x}_k) + \log(1 - D_\psi(G_\theta(\mathbf{z})))$ ;
    Sample  $\delta_i, \delta_j \sim \mathcal{N}(0, \sigma \mathbf{I}_d)$  i.i.d.;
     $\mathbf{z}_i^* \leftarrow \mathbf{z}^*(\mathbf{y}_i) + \delta_i$ ;
     $\mathbf{z}_j^* \leftarrow \mathbf{z}^*(\mathbf{y}_j) + \delta_j$ ;
     $L^{rec} \leftarrow \frac{1}{2}(F(G_\theta(\mathbf{z}_i^*), \mathbf{y}_i) + F(G_\theta(\mathbf{z}_j^*), \mathbf{y}_j))$ ;
    Sample  $\alpha \sim U[0, 1]$ ;
     $\mathbf{z}_{ij}^* = \alpha \mathbf{z}_i^* + (1 - \alpha) \mathbf{z}_j^*$ ;
     $L^{itp} \leftarrow \alpha F(G_\theta(\mathbf{z}_{ij}^*), \mathbf{y}_i) + (1 - \alpha) F(G_\theta(\mathbf{z}_{ij}^*), \mathbf{y}_j)$ ;
     $L \leftarrow L^{adv} + \lambda L^{rec} + \beta L^{itp}$ ;
     $\psi = \psi + \eta \nabla_\psi L$ ;
     $\theta = \theta - \eta \nabla_\theta L$ ;
  end
end

```

6 Supplementary material

A Algorithm

To support the readability and reproducibility of our IMLE-GAN method with minority inclusion (described in Section 3.3), we summarize it as an algorithm in Algorithm 1, where E is the number of training epochs, S indicates how often (in epochs) to update latent matching, m is the pool size of the latent vector candidates, δ_i, δ_j are the additive Gaussian perturbations (with variance σ^2) to the matching latent vectors for better generalization, λ and β are used to balance each loss term, and η is the learning rate. We provide more information on the hyperparameters below.

B Hyperparameter Settings

IMLE-GAN. We train each model using Adam optimizer [25] for $K = 300$ epochs. The learning rate $\eta = 0.002$, the same as in StyleGAN2 [24]. We update the matching of latent vectors to data points every $S = 20$ epochs. The size of the pool of latent vector candidates is 10 times of the size of the dataset or the minority group depending on the application. Perturbation variance is $\sigma^2 = 0.05^2$. The weight of the reconstruction loss varies according to the choice of metric, such that the magnitude of the reconstruction loss is about equal

to that of the adversarial loss. For ℓ_2 distance in pixel space, $\lambda = 36$. In the discriminator feature space [27] $\lambda = 9.6 \times 10^6$. In the Inception feature space [19] $\lambda = 10$. For LPIPS [52] $\lambda = 2.5$. Consistently, the weight of the interpolation loss is always set to $\beta = 0.4\lambda$.

Baseline methods. For fair comparisons, all the baseline methods are re-implemented using the same StyleGAN2 backbone and training strategies. For DSGAN [46], we tune the weight of the diversity regularization term such that its value is about 1/4 of the adversarial loss. For PacGAN [32], we set the pack size to 8. For VAEGAN [27], we tune the weights of the data reconstruction term and the prior term such that the former is about equal to the adversarial loss and the latter is about 1/4 of that. For VEEGAN [42], we tune the weight of the latent reconstruction term such that its value is about equal to the adversarial loss. For SNGAN [36] and ALI [11], there is no additional hyperparameter.

Evaluation. For Precision and Recall [39] measurement, we use the default setting from their official code repository. In particular, the features are extracted from the *Pool3* layer of a pre-trained Inception network [19]. The number of clusters for *k*-means is set to 20. We launched for 10 independent runs and report the average for Precision and Recall. For IvOM [35] measurement, the similarity metric is based on LPIPS [52]. Given each query image and a learned generative model, we optimized the latent vector via Adam [25] for 400 steps. The learning rate setting strategy is the same as in StyleGAN2: the maximum learning rate is 0.1, and it is ramped up from zero linearly during the first 20 steps and ramped down to zero using a cosine schedule during the last 100 steps.

C Additional Results on Minority Inclusion

In order to dynamically demonstrate the effectiveness of our minority inclusion models, we are attaching four videos at GitHub. The videos show the results of interpolating in the latent space from one arbitrary image to another image with specific attribute(s). In this way we show our minority inclusion model variants perform comparably to the other models for majority groups, and outperform the others for minority groups. In each video, the leftmost column is an arbitrary real image and the rightmost column is an arbitrary real image with specific attribute(s) of interest. For each generative model, we project the image in the leftmost column onto its latent space (i.e.: we find the latent vector that results in a generated image that is most perceptually similar to the image according to LPIPS [52]), and then interpolate starting from this latent vector. We do the same for the image in the rightmost column and use the resulting latent vector as the target for interpolation. The sub-videos in the middle three columns are the images produced by three methods: StyleGAN2 [24], our general IMLE-GAN model described in Section 3.3 and 4.5 (“Ours LPIPS interp”), and our IMLE-GAN model with specific minority inclusion described in Section 3.4 and 4.6 (Ours *attributeA&attributeB*). The four videos correspond to the four arbitrarily selected attributes or attribute combinations used in Section 4.6: *Eyeglasses*, *Bald*, *Narrow.Eyes&Heavy_Makeup (NE&HM)*, and *Bags_Under_Eyes&High_Cheekbone&Attractive (BUE&HC&A)*. For convenience, we show the last frame of each video in Figure 6, where each generated image

is the projection of the rightmost image (a real image from the minority group) onto the space of images learned by each generative model.

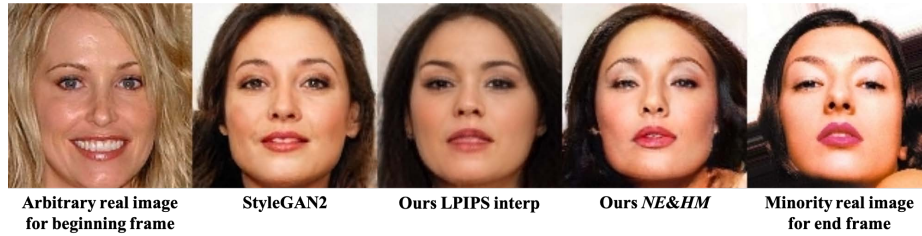
We note from the qualitative comparisons that incorporating minority inclusion in the training objective ensures coverage of the specified minority group, with little or no compromise from their performance on the majority. For example, in each video, at the beginning the three models are comparably representative for the arbitrary real image from the majority group (the leftmost column). As the latent vector transitions towards the corresponding minority region (the rightmost column), the attribute appearances of the minority group are not reconstructed accurately by the two models without an explicit focus on minority attributes (the second and third columns from the left). On the contrary, our minority inclusion model (the second column from the right) effectively represents the desired minority attributes, e.g., sunglasses, narrow eye shapes, or eye bags.



(a) Minority: *Eyeglasses*



(b) Minority: *Bald*



(c) Minority: *Narrow_Eyes&Heavy_Makeup*



(d) Minority: *Bags_Under_Eyes&High_Cheekbone&Attractive*

Fig. 6. The last frame of each video at GitHub. Each of the middle three columns denotes a generated image from a learned model, the latent vector of which is projected from the image in the rightmost column (a real image from one minority subgroup).